Benchmarking Hydrogen Evolving Reaction and Oxygen Evolving Reaction Electrocatalysts for Solar Water Splitting Devices

Charles C. L. McCrory,*,[†,‡] Suho Jung,[†,‡] Ivonne M. Ferrer,[†,‡] Shawn M. Chatman,[†,‡] Jonas C. Peters,*,[†,‡] and Thomas F. Jaramillo*,[†,§]

[†]Joint Center for Artificial Photosynthesis and [‡]Division of Chemistry and Chemical Engineering, California Institute of Technology, Pasadena, California 91125, United States

[§]Department of Chemical Engineering, Stanford University, Stanford, California 94305, United States

Ⓢ *Supporting Information*

ABSTRACT: Objective comparisons of electrocatalyst activity and stability using standard methods under identical conditions are necessary to evaluate the viability of existing electrocatalysts for integration into solar-fuel devices as well as to help inform the development of new catalytic systems. Herein, we use a standard protocol as a primary screen for evaluating the activity, short-term (2 h) stability, and electrochemically active surface area (ECSA) of 18 electrocatalysts for the hydrogen evolution reaction (HER) and 26 electrocatalysts for the oxygen evolution reaction (OER)

under conditions relevant to an integrated solar water-splitting device in aqueous acidic or alkaline solution. Our primary figure of merit is the overpotential necessary to achieve a magnitude current density of 10 mA cm^{-2} per geometric area, the approximate current density expected for a 10% efficient solar-to-fuels conversion device under 1 sun illumination. The specific activity per ECSA of each material is also reported. Among HER catalysts, several could operate at 10 mA cm^{-2} with overpotentials <0.1 V in acidic and/or alkaline solutions. Among OER catalysts in acidic solution, no non-noble metal based materials showed promising activity and stability, whereas in alkaline solution many OER catalysts performed with similar activity achieving 10 mA cm^{-2} current densities at overpotentials of ∼0.33−0.5 V. Most OER catalysts showed comparable or better specific activity per ECSA when compared to Ir and Ru catalysts in alkaline solutions, while most HER catalysts showed much lower specific activity than Pt in both acidic and alkaline solutions. For select catalysts, additional secondary screening measurements were conducted including Faradaic efficiency and extended stability measurements.

INTRODUCTION

The identification of efficient electrocatalysts comprised of earth-abundant materials for the oxygen evolution reaction (OER) and the hydrogen evolution reaction (HER) is crucial for the development of solar water-splitting devices.[1−10] In particular, the discovery of new electrocatalytic materials for water-splitting reactions is a prominent and growing field of research. An examination of the literature shows that hundreds of electrocatalytic systems for HER and OER have been reported with numerous different elemental compositions and microstructures prepared in a variety of ways.[9−15] This number will likely increase dramatically in coming years due to the expanded use of high-throughput combinatorial techniques for the discovery of new OER and HER catalysts in various ternary and quaternary composition spaces.[16−23] However, reliable methods for measuring and reporting the performance of these materials under identical conditions have not been uniformly applied, complicating meaningful comparisons of the catalytic activity and stability of these systems. There is a need for standardization in the evaluation of catalytic performance for OER and HER systems to evaluate the utility of existing catalysts for device integration, provide experimental evidence

to aid or corroborate theoretical models of catalyst systems,[24,25] and highlight existing technological gaps to help inform the development of new catalyst materials.

We have previously reported a benchmarking protocol to measure the activity, stability, and Faradaic efficiency of a series of representative OER catalysts in acidic and alkaline solution.[26] This protocol was specifically developed to allow for the rapid screening of electrocatalytic performance using standard electrochemical procedures and equipment easily accessible to a typical researcher in the field of electrocatalysis. Absent from the previous study was the evaluation of HER catalysts, a critical need for the identification of active and stable catalysts for integrated water-splitting devices. Herein, we have further established the viability of this benchmarking methodology as a primary screen for HER catalyst performance by evaluating 16 HER non-noble metal electrocatalysts (Table 1) under conditions relevant to an integrated artificial photosynthetic device under 1 sun illumination in 1 M NaOH or 1 M H$_2$SO$_4$.

Table 1. Catalysts Investigated in Benchmarking Study[a]

HER catalyst	elements from XPS[c]	ref	OER catalyst[b]	elements from XPS[c]	ref
Co-(a)	Co, Na, Cl	34	Co-(b)	Co, Na	35
CoMo	Co, Mo	36	Co/B	Co, K, B	37
CoNiFe	Co, Ni, Fe, Na, Cl	38	Co/P-(a)	Co, K, P	39
CoW	Co, W, Na	36	Co/P-(b)	Co, Na, P	40
Fe-(a)	Fe	41	CoFe	Co, Fe, S	35
FeMo	Fe, Mo, Na	42	Cu	Cu	35
Mo/S	Mo, S, Na	43, 44	Fe-(b)	Fe, S	35
Ni-(a)	Ni, S, Na	41	FeMn	Fe, Mn	35
NiCo-(a)	Ni, Co, Na	45	Ir	Ir	33
NiFe-(a)	Ni, Fe, Cl	41	Ni-(b)	Ni	46
NiMo-(a)	Ni, Mo, Na	36, 47	Ni/B	Ni, B	48
NiMo-(b)	Ni, Mo, Na, K, P	49	NiCe	Ni, Ce, N	46
NiMoCo	Ni, Mo, Co	50	NiCo-(b)	Ni, Co, N	46
NiMoFe-(a)	Ni, Mo, Fe, Na, K	51	NiCo-(c)	Ni, Co, B, S	52
NiSn-(a)	Ni, Sn, K, Cl	53	NiCr	Ni, Cr, S	54
NiW-(a)	Ni, W, Na, K	45, 47	NiCu	Ni, Cu, N	46
Pt-(a)	Pt	–	NiFe-(b)	Ni, Fe, S	35
Pt-(b)	Pt, Cl	55	NiFe-(c)	Ni, Fe	56
			NiFeCoCe-(a)	Ni, Fe, Co, Ce[d]	23
			NiFeCoCe-(b)	Ni, Fe, Co, Ce[d]	23
			NiLa	Ni, La, N	46
			NiMoFe-(b)	Ni, Fe, Mo, Na, K, S	57
			NiSn-(b)	Ni, Sn, K, Cl, P, N	58
			NiZn	Ni, K[e]	58
			Ru-(a)	Ru	59
			Ru-(b)	Ru	33

[a]Because quantitative analysis of the surface composition of each catalyst during operation is beyond the scope of this manuscript, only the metal components of each catalyst are used for naming the materials. Exceptions are made for materials for which the reported composition by which the material is known includes a nonoxide anion (e.g., MoS_x = Mo/S, CoP_i = Co/P-(a), CoP = Co/P-(b), etc.). [b]The various catalysts shown for OER are assumed to form surface oxides under oxidative conditions. However, because we do not measure the quantitative surface-composition during operation and several systems are argued to incorporate nonoxide anions into the catalytic surface layer, we chose not to make any suggestion of oxide surface stoichiometry and instead listed the OER catalysts using the same naming protocol as with the HER materials. [c]The listed elements are based on the assigned peaks from the XPS spectra in Figures S21−S62. C and O are not listed, but are present in every sample. Si is also not listed, although it is present in some samples due to residual SiC from the electrode polishing procedures. No effort was made to distinguish whether nontransition metal elements such as Na, K, Cl, B, N, P and S are incorporated into the film or simply from adsorbed ions on the material surface. [d]The elemental composition listed here is based on previously reported EDX and XPS characterization.[23] [e]The lack of Zn in the XPS spectra is likely due to Zn dissolution during the postelectrodeposition 24 h immersion in 28% KOH.

Additionally, we have expanded the number of OER catalysts evaluated from the previous study to include 23 non-noble metal electrocatalysts (Table 1). A Pt disk electrode and platinized Pt electrode were also investigated as HER standards,

and a sputtered Ir catalyst and 2 different deposited Ru catalysts were investigated as OER standards. The primary figure of merit is the overpotential necessary to achieve a magnitude current density per geometric area $|j|$ = 10 mA cm^{-2}, the approximate current density expected for an integrated solar water-splitting device under 1 sun illumination operating at 10% solar-to-fuels efficiency.[9,27,28] The current manuscript provides one of the most comprehensive, self-consistent studies of the activity and stability of HER and OER catalysts.

For selected catalysts, a secondary screen was used to evaluate the Faradaic efficiency and longer-term, 24 h stability of 12 OER catalysts in 1 M NaOH and 5 HER catalysts in 1 M H_2SO_4 and 5 HER catalysts in 1 M NaOH. In particular, the NiMo-(a) HER catalyst showed remarkable activity and 24 h stability under constant polarization in 1 M H_2SO_4, warranting a tertiary screen of catalyst stability using rapid potential cycling for 10 000−40 000 cycles.

■ EXPERIMENTAL SECTION

Materials. All reagents were purchased from commercial sources and in analytical or reagent grade when possible. A full list of chemicals used including the vendor and reported purity can be found in the Supporting Information. All water used was purified using a Thermo Scientific Barnstead Nanopure water purification system (18.2 MΩ·cm resistivity). Oxygen (O_2, Alphagaz-1 grade 99.999%) and hydrogen (H_2, Alphagaz-1 grade, 99.999%) were purchased from Air−Liquide. Nitrogen (N_2) was boil-off gas from a liquid nitrogen source. All gases were water-saturated by bubbling through a gas washing bottle filled with water.

Analytical Equipment. All electrochemical measurements were conducted with a Bio-Logic VMP3 multichannel potentiostat/galvanostat with a built-in EIS analyzer. The working electrodes were 5 mm diameter disk electrodes with a surface area of 0.196 cm^2. The working electrodes were mounted in a Pine Instrument Company E6-series ChangeDisk rotating disk electrode (RDE) assembly in an MSR rotator. The auxiliary electrodes were carbon rods (99.999%, Strem Chemicals), and the reference electrode was a commercial saturated calomel electrode (SCE) (CH Instruments) that was externally referenced to a solution of ferrocene carboxylic acid (Sigma-Aldrich) in a 0.2 M phosphate buffer at pH 7 (0.284 V vs SCE).[29] All data were recorded using the Bio-Logic EC-Lab software package.

X-ray photoelectron spectroscopy (XPS) analysis was conducted using a Kratos Axis Nova spectrometer with DLD (Kratos Analytical). The excitation source for all analysis was monochromatic Al K$\alpha_{1,2}$ ($h\nu$ = 1486.6 eV) operating at 30 mA and 15 kV. The X-ray source was directed 45° with respect to the sample normal. A base pressure of 1 × 10^{-9} Torr was maintained in the analytical chamber, which rises to 5 × 10^{-9} Torr during spectral acquisition. All spectra were acquired using the hybrid lens magnification mode and slot aperture, resulting in an analyzed area of 700 μm × 400 μm. Survey scans (0−1200 eV) were collected using 160 eV pass energy, and higher-resolution scans (270−340 eV) used 20 eV pass energy. XPS data analysis was performed using CasaXPS version 2.3.16 (Casa Software Ltd.; Teignmouth, UK), and XPS survey peaks were assigned using the CasaXPS software package, the NIST X-ray Photoelectron Spectroscopy Database,[30] and the PerkinElmer Handbooks of X-ray Photoelectron Spectroscopy.[31,32]

Electrode Preparation and Catalyst Deposition. Catalysts were deposited onto 5 mm diameter, 4 mm thick Sigradur G glassy carbon (GC) disks (HTW Hochtemperatur-Werkstoff GmbH). Prior to deposition, the GC disks were first polished with 600 grit Carbimet SiC grinding paper (Buehler) on a Struers LaboPol-5 polishing wheel at 200 rpm for 1 min and sonicated briefly in ~1.5 M HNO$_3$ for 1 min. The disks were then sequentially polished with 9, 6, 3, 1, and 0.1 μm MetaDi Supreme diamond slurries (Buehler) with an MD-Floc synthetic nap polishing pad (Struers) on a Struers LaboPol-5 polishing wheel at 200 rpm for 30 s, then sonicated for 10 min in pure water, 5 min in acetone, 5 min in isopropanol, and 10 min again in pure water.

Pt disks (Pt-(a)) were polished in an analogous manner to that used for the GC disks. Polishing and grinding pads used for the preparation of Pt disk were kept separate from those used to prepare GC disks to prevent possible cross-contamination. Platinized Pt electrodes (Pt-(b)) were prepared by polarizing polished Pt disk electrodes at −50 mA cm^{-2} for 1 min in a solution of 0.052 g of chloroplatinic acid hydrate in 5 mL of 0.1 M HCl in water.

A list of all HER and OER catalyst investigated in this study is shown in Table 1. Note that for the purposes of catalyst identification in this manuscript, we list only the metal components of each system (as confirmed by XPS survey scans). Exceptions to this general naming protocol are made for materials for which the reported composition by which the material is known includes a nonoxide anion (e.g., MoS_x = Mo/S, NiB_i = Ni/B, etc.). We use this naming protocol even for the OER catalysts, which we can safely assume form surface oxides under OER conditions. However, measuring the quantitative surface composition during operation is beyond the scope of this study, and several systems are argued to incorporate nonoxide anions into the catalytic surface layer forming nonsimple oxide surfaces. For these reasons, we chose not to make any suggestion of oxide surface stoichiometry and instead list both OER and HER catalysts using the same naming protocol.

The deposition conditions for each electrodeposited catalyst were adapted from literature procedures and are summarized in Tables S1−S2. Each electrodeposition was conducted in a 100 mL cell with 40 mL of deposition solution, and the auxiliary electrode was separated from the working and reference electrodes using a fine-porosity glass frit (BioAnalytical Systems, Inc.). When applicable, pH measurements of deposition solutions were conducted with a VWR Symphony multiparameter meter with a Thermo Scientific Orion refillable Ag/AgCl pH electrode filled with Orion Ag/AgCl reference electrode filling solution. The pH meter was calibrated with a 5 point calibration curve at pH = 1.68, 4.00, 7.00, 10.00, and 12.45.

In addition to the electrodeposited catalysts, several catalyst systems were deposited via other methods. Ir and Ru-(b) were sputtered directly onto glassy-carbon electrode disks based on a reactive-sputtering method adapted from a previously reported procedure.[33] Glassy-carbon electrode disks were affixed to a glass slide using double-sided Kapton tape, and then Ir and Ru were sputtered on the electrode surface from an RF source at 200 W at 300 °C for 30 min under a constant flow of 3.0/3.0 sccm Ar/O_2 for Ir and 4.5/0.5 sccm Ar/O_2 for Ru-(b) using Ir and Ru targets, respectively (≥99.9% from AJA International). Moreover, NiFeCoCe-(a) ($Ni_{0.5}Fe_{0.3}Co_{0.17}Ce_{0.03}O_x$) and NiFeCoCe-(b) ($Ni_{0.3}Fe_{0.07}Co_{0.2}Ce_{0.43}O_x$) were inkjet-printed directly onto GC electrodes from metal precursor inks as previously described,[23] and were evaluated for OER in alkaline solution.

Electrochemical Measurements. All activity, stability, and surface area measurements were conducted in a modified 2-chamber U-cell in which the first chamber held the working and reference electrodes in ∼150 mL of solution and the second chamber held the auxiliary electrode in ∼25 mL of solution as previously described.[26] The two chambers were separated by a fine-porosity glass frit. The cell was purged for ∼30 min with O_2 or H_2 prior to each set of experiments. For the static voltammetry measurements, the solution was blanketed under O_2 or H_2 during the measurement. During rotating disk electrode (RDE) measurements, the solution in the working electrode chamber was continuously bubbled with O_2 or H_2. The uncompensated resistance was measured with a high-frequency impedance measurement at 100 kHz with 20 mV amplitude about the open-circuit potential (OCP). Cyclic voltammetry and chronoamperometry measurements were corrected for IR drop at 85% using the Biologic EC-Lab software. Chronopotentiometry measurements were manually corrected for IR drop. Our typical electrochemical setup resulted in R_u = ∼6 Ω in 1 M H_2SO_4 and R_u = ∼10 Ω in 1 M NaOH.

Electrochemical capacitance was determined using cyclic voltammetry (CV) measurements.[26] The potential range where there is a non-Faradaic current response was determined from CV. This range is typically a 0.1 V window centered at OCP of the system. CV measurements were conducted in quiescent solution by sweeping the

potential across the non-Faradaic region from the more positive to more negative potential and back at 8 different scan rates: 0.005, 0.01, 0.025, 0.05, 0.1, 0.2, 0.4, and 0.8 V s^{-1}. The working electrode was held at each potential vertex for 10 s before beginning the next sweep.[26,60]

Faradaic Efficiency. For Faradaic efficiency measurements, dissolved O_2 and H_2 was quantified using Unisense Ox-500 oxygen probe and H2-500 hydrogen probes, respectively, controlled by a Unisense Microsensor Multimeter. The Ox-500 oxygen probe was calibrated with a 3 pt calibration in O_2-saturated, air-saturated (20.8% O_2), and N_2-sparged solution. The H2-500 hydrogen probe was calibrated with a 2 pt calibration in H2-saturated and N_2-sparged solution. The saturation concentration of dissolved H_2 at 20 °C in 1 M H_2SO_4 and 1 M NaOH were calculated using the empirical gas solubility model by Weisenberg and Schumpe[61] to be $[H_2]_{saturated}$ = 0.72 mM in 1 M H_2SO_4 and 0.56 mM in 1 M NaOH. The saturation concentrations of dissolved O_2 at 20 °C were determined from linear interpolation of solubility data reported at 15 and 25 °C: $[O_2]_{saturated}$ = 1.04 mM in 1 M H_2SO_4 and 0.83 mM in 1 M NaOH.[62,63]

Faradaic efficiency measurements were conducted in a custom-built two-compartment cell (Figure S1). The first compartment was gastight and housed the working electrode, reference electrode, and either the hydrogen or oxygen probe with a total volume of 73 mL. The second compartment housed the carbon-rod auxiliary electrode, and the two compartments were separated by a 0.007 in. thick Nafion-117 membrane (Sigma-Aldrich). Both compartments were filled with electrolyte, and the first compartment was filled such that there was no appreciable headspace. For H_2-measurements, the solution was sparged for ∼30 min with N_2 under vigorous stirring. For O_2-measurements, the solution was air-saturated prior to use.

The concentration of dissolved gas was monitored for 1 min at open circuit, and then the working electrode was held at a magnitude current density of |j| = 10 mA cm^{-2} for 15 min passing a total of 1.755 C of charge for H_2 measurements and 30 min passing a total of 3.510 C charge for O_2 measurements. The increase in dissolved gas concentration was monitored during this time, and from this the total amount of O_2 or H_2 produced was determined. The amount of measured O_2 or H_2 was then divided by the amount calculated from the total charge passed to determine the Faradaic efficiency.

RESULTS AND DISCUSSION

Benchmarking Measurement Protocol. The protocol used in the current study shown in Figure 1 is adapted from one that has been previously described in detail.[26] The specific measurements conducted in this study are briefly outlined below. The benchmarking protocol used was designed to evaluate and compare the performance of OER and HER electrocatalysts under conditions relevant to an integrated solar water-splitting device under 1 sun illumination with moderate throughput.

The qualitative elemental composition of each catalyst was determined from XPS survey scans from 0 to 1200 eV binding energy. To test for the unexpected presence of noble metals, high-resolution scans between 270 and 340 eV binding energy were taken of each surface and investigated for the presence of photoemission originating from Pt_{4d}, Ir_{4d}, and Ru_{3d}. In general, no peaks associated with any noble metals were observed except when evaluating Ru, Ir, and Pt catalysts. The XPS analysis suggests there is no noble-metal contamination in the non-noble metal electrodeposited catalysts within the ∼0.1 atom % detection limit of XPS.[64,65]

The electrochemically active surface area (ECSA) and roughness factor (RF) of each catalyst were estimated by determining the double-layer capacitance of the system from CV. First, a non-Faradaic potential range was identified from CV in quiescent solution. This non-Faradaic region is typically a 0.1 V window about OCP, and all measured current in this
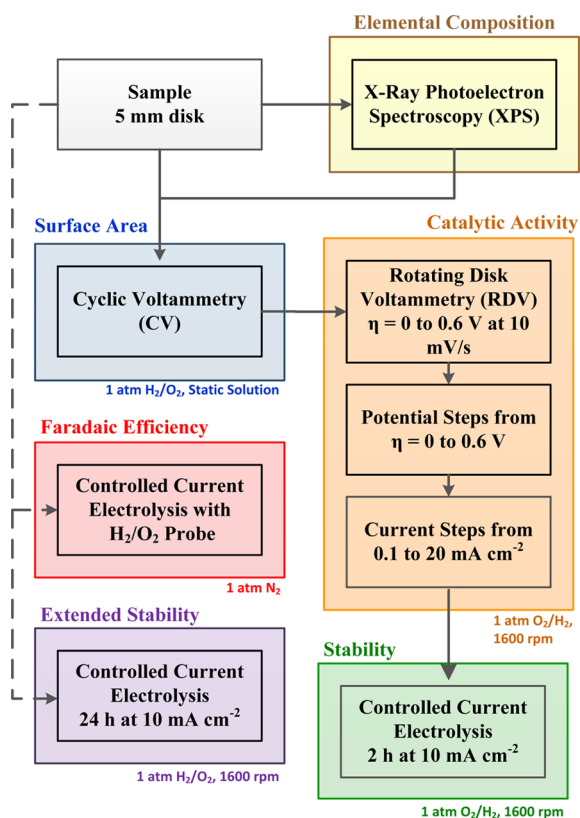
Figure 1. Protocol for benchmarking the performance of heterogeneous electrocatalysts for HER and OER.

region is assumed to be due to double-layer charging. Based on this assumption, the charging current, i_c, is equal to the product of the electrochemical double layer capacitance, C_{DL}, and the scan rate, ν, as shown in eq 1.[60,66−68]

$$i_c = \nu C_{DL} \tag{1}$$

Plotting i_c as a function of ν yields a straight line with slope equal to C_{DL}. Representative samples of C_{DL} measurements for NiMo-(a) and Co-(b) are shown in Figures S2−S5.

The electrochemically active surface area (ECSA) of the catalyst can be calculated by dividing C_{DL} by the specific capacitance of the sample as shown in eq 2.

$$\text{ECSA} = \frac{C_{DL}}{C_S} \tag{2}$$

Here we use a general specific capacitance of 0.035 mF cm^{-2} in 1 M H$_2$SO$_4$ and 0.040 mF cm^{-2} in 1 M NaOH. The choice of specific capacitance is based on typical values reported for metal electrodes in aqueous H$_2$SO$_4$ and NaOH solutions as previously described.[26] The roughness factor (RF) is then calculated by dividing ECSA by 0.196 cm^2, the geometric area of the electrode. The RF values determined for each material are summarized in Tables S3−S6, and for select catalysts in Table 2. Note that the standard deviations reported for the RF measurements do not necessarily reflect the accuracy of the determined RF, but instead are an indication of the precision of the measurements. In general, we believe the accuracy of the RF measurements within about an order of magnitude,[26] and emphasize that the values should be considered only as an approximate guide for comparing electroactive surface area.

The catalytic activity of each system was measured using a combination of rotating-disk electrode (RDE) voltammetry measurements at 0.01 V s^{-1} scan rate, 30 s controlled current chronopotentiometric steps, and 30 s controlled potential chronoamperometric steps all at 1600 rpm rotation rate. Representative RDE voltammograms for NiMo-(a) and Co-(b) along with steady-state currents determined from potential and current step measurements are shown in Figures S6−S9. The primary figure of merit for this study is the overpotential necessary to achieve a magnitude current density |j| = 10 mA cm^{-2} per geometric area. The resulting measurements of the overpotentials necessary to achieve |j| = 10 mA cm^{-2} at time = 0 ($\eta_{t=0}$) and at time = 2 h ($\eta_{t=2h}$) are summarized for every catalyst investigated in Tables S3−S6, and for select catalysts in Table 2.

A graphical representation of the relevant benchmarking parameters for OER and HER catalysts in 1 M H$_2$SO$_4$ and 1 M NaOH is shown in Figure 2. The x-axis represents the magnitude of the overpotential necessary to achieve |j| = 10 mA cm^{-2} at t = 0, our primary figure of merit for catalytic activity. The y-axis represents the magnitude of the overpotential necessary to achieve |j| = 10 mA cm^{-2} after 2 h of constant polarization at 10 mA cm^{-2}, a primary measure of short-term catalyst stability. A diagonal dashed black line represents the expected response for a stable catalyst that shows the same activity at t = 0 and t = 2 h. The color of each point represents the roughness factor of the catalyst with a bin size of 1 order of magnitude, approximately the estimated accuracy of our surface-area measurements.[26] The size of each point is inversely proportional to the standard deviation in the RF measurements. The best catalyst materials should operate with low over-potentials and have high specific activity (and therefore low surface area), and thus they will appear toward the bottom left of each plot and would ideally be light-green in color. Zoomed-in regions of the graphical representation for HER in 1 M NaOH and 1 M H$_2$SO$_4$ between 0 and 0.3 V and OER in 1 M NaOH between 0.28 and 0.5 V are shown in Figure 3.

In general, the target combined overpotential for OER and HER in a 10% efficient integrated solar water-splitting device should be |η| < 0.45 V according to previously reported device models.[9,27,69,70] Accordingly, we propose that a reasonable HER catalyst should operate at |j| = 10 mA cm^{-2} at |η| ∼ 0.1 V, leaving |η| ∼ 0.35 V available for OER at 10 mA cm^{-2}. Thus, our primary region of interest is defined by |$\eta_{t=0}$| = |$\eta_{t=2h}$| < 0.1 V for HER and |$\eta_{t=0}$| = |$\eta_{t=2h}$| < 0.35 V for OER. The boundaries of this region are shown as dashed blue lines in Figure 2. The current density per geometric area of each OER and HER catalyst at η = 0.35 V and η = −0.10 V, respectively are summarized in Tables S3−S6.

In addition, the average specific current density, j_s, of each catalyst normalized for ECSA at η = 0.35 V for OER and η = −0.10 V for HER are also summarized in Tables S3−S6, and for select catalysts in Table 2. Here, the specific activity is calculated by dividing the current density per geometric area at η = 0.35 V by the determined roughness factor. The standard errors reported along with the j_s values are calculated from the standard deviations in the measurements of the RF and current density per geometric area, and are indicative of the precision of the measurements. Due to the inherent inaccuracies in determining RF, we caution that j_s values do not supplant $\eta_{t=0}$ as a primary figure of merit for catalytic activity, and should instead be used as an approximate guide in comparing specific activity. In particular, a recent report has investigated the OER

Table 2. Relevant Benchmarking Parameters for Select HER and OER Catalysts^a

catalyst	RF	$\eta_{t=0}$ (V)	$\eta_{t=2h}$ (V)	$\eta_{t=24h}$ (V)	$|j_s|$ (mA cm^{-2}) (ECSA)^b	ε
			HER in 1 M H$_2$SO$_4$			
CoMo	1100 ± 600	-0.10 ± 0.02	-0.10 ± 0.01	-0.09 ± 0.02	0.004 ± 0.003	0.99 ± 0.08
NiMo-(a)	1200 ± 500	-0.045 ± 0.004	-0.039 ± 0.003	-0.030 ± 0.002	0.074 ± 0.048	0.96 ± 0.03
NiMo-(b)	1000 ± 500	-0.11 ± 0.02	-0.12 ± 0.02	-0.12 ± 0.03	0.007 ± 0.005	0.99 ± 0.03
NiMoCo	1200 ± 500	-0.05 ± 0.01	-0.05 ± 0.01	-0.04 ± 0.01	0.043 ± 0.028	0.93 ± 0.03
NiW	1200 ± 600	-0.06 ± 0.02	-0.11 ± 0.05	-0.33 ± 0.06	0.014 ± 0.011	1.00 ± 0.03
			HER in 1 M NaOH			
CoMo	700 ± 400	-0.10 ± 0.02	-0.10 ± 0.02	-0.10 ± 0.02	0.014 ± 0.008	0.92 ± 0.02
NiMo-(a)	800 ± 400	-0.04 ± 0.02	-0.03 ± 0.01	-0.03 ± 0.02	0.047 ± 0.038	0.93 ± 0.08
NiMo-(b)	1000 ± 700	-0.07 ± 0.02	-0.10 ± 0.03	-0.13 ± 0.03	0.020 ± 0.014	0.90 ± 0.04
NiMoCo	900 ± 400	-0.07 ± 0.03	-0.09 ± 0.04	-0.11 ± 0.05	0.020 ± 0.015	0.93 ± 0.02
NiW	900 ± 500	-0.20 ± 0.03	-0.20 ± 0.05	-0.21 ± 0.01	0.002 ± 0.001	0.91 ± 0.07
			OER in 1 M H$_2$SO$_4$			
Ru-(a)	71 ± 8	0.28 ± 0.03	0.34 ± 0.05	0.82 ± 0.40^c	0.42 ± 0.13	0.92 ± 0.04
Ir	160 ± 20	0.34 ± 0.01	0.36 ± 0.02	0.44 ± 0.02	0.09 ± 0.03	0.93 ± 0.04
			OER in 1 M NaOH			
Co-(b)	11 ± 5	0.41 ± 0.03	0.40 ± 0.04	0.81 ± 0.43^c	0.05 ± 0.04	0.97 ± 0.01
Co/P-(a)	17 ± 9	0.39 ± 0.02	0.38 ± 0.02	0.35 ± 0.02	0.04 ± 0.03	0.91 ± 0.05
Co/P-(b)	80 ± 50	0.38 ± 0.02	0.36 ± 0.02	0.34 ± 0.02	0.04 ± 0.03	0.92 ± 0.05^d
CoFe	10 ± 3	0.35 ± 0.01	0.36 ± 0.01	0.36 ± 0.03	0.53 ± 0.24	0.98 ± 0.03
Ni-(b)	2 ± 1	0.47 ± 0.04	0.47 ± 0.03	1.23 ± 0.06	0.34 ± 0.23	0.90 ± 0.02
NiCo-(b)	3 ± 2	0.42 ± 0.02	0.42 ± 0.03	1.17 ± 0.32	0.31 ± 0.21	0.91 ± 0.05
NiCo-(c)	9 ± 4	0.38 ± 0.01	0.35 ± 0.01	0.34 ± 0.01	0.24 ± 0.14	0.92 ± 0.02
NiCr	9 ± 3	0.39 ± 0.02	0.39 ± 0.02	0.79 ± 0.45^c	0.20 ± 0.12	0.90 ± 0.04
NiFe-(b)	4 ± 1	0.34 ± 0.02	0.37 ± 0.02	0.37 ± 0.03	2.78 ± 1.65	0.93 ± 0.02
NiMoFe-(b)	9 ± 3	0.34 ± 0.02	0.33 ± 0.02	0.32 ± 0.01	2.1 ± 1.4	0.97 ± 0.05
NiZn-(b)	200 ± 100	0.36 ± 0.02	0.35 ± 0.03	0.34 ± 0.03	0.03 ± 0.02	0.90 ± 0.05
Ru-(a)	70 ± 20	0.29 ± 0.03	0.32 ± 0.02	0.36 ± 0.02	0.49 ± 0.24	0.93 ± 0.07

^{a}Values reported are averages from at least 3 measurements with standard deviations. ^{b}Measured at $\eta = -0.1$ V for HER, and $\eta = 0.35$ V for OER. Note that the standard errors reported along with the j_s values are calculated from the standard deviations in the measurements of the RF and current density per geometric area, and are indicative of the precision of the measurements. ^{c}Ru-(a) in H$_2$SO$_4$ and Co-(b) and NiCr in NaOH showed variable 24 h stability in multiple (7) experiments. Chronopotentiometric data shows a catastrophic (rather than gradual) loss of catalytic activity occurring at times greater than $\sim$16 h. Representative 24 h chronopotentiometric data are shown in Figures S15–S17. ^{d}Faradaic efficiency measured after holding the electrode at 10 mA cm^{-2} for 24 h. The Faradaic efficiency measured for the electrodeposited material before the 24 h activation is 0.70 ± 0.05.

specific current density in 0.1 M KOH per oxide-surface area for the (110) and (100) orientations of smooth, pulse-laser deposited films of Ir and Ru on (001)-oriented SrTiO$_3$.[71] The reported specific current densities at $\eta = 0.35$ V for the RuO$_2$(110) ($j_{s,RuO_2} \sim 0.4$ mA cm$^{-2}_{ox}$) and IrO$_2$(100) ($j_{s,IrO_2} \sim 0.03$ mA cm$^{-2}_{ox}$) surfaces match closely to the specific current densities measured in this study for Ru-(a) ($j_{s,Ru-(a)} = 0.5 \pm 0.2$ mA cm^{-2}) and Ir ($j_{s,Ir} = 0.022 \pm 0.005$ mA cm^{-2}) in 1 M NaOH (Table S6).

Note that the specific activity for Ru-(b) is somewhat lower than that for Ru-(a) and RuO$_2$(110) with $j_s = 0.09 \pm 0.04$ mA cm^{-2}. Sputtered Ru films such as Ru-(b) are known to be nanoporous,[33] which helps to account for its relatively high roughness factor. However, slow mass-transport of OH$^-$ into and O$_2$ out of porous electrodes can cause interior active sites within the porous film to become catalytically inaccessible during OER operation. Any loss of accessibility to interior active sites would result in a lower calculated specific activity for the Ru-(b) film.

While the close correlation between the measured j_s values for Ru-(a) and Ir compared to previously reported values for planar surfaces lend credibility to the use of ECSA measurements in calculating specific activity, the results for Ru-(b) highlight a fundamental limitation of the approach when

considering nanostructured and porous films. We again emphasize that any use of j_s values calculated from ECSA should be used as an approximate guide for comparing specific activity and should not be interpreted as an absolute reflection of turnover frequency, especially when comparing high-surface area and/or nanoporous films.

For particularly active catalysts, additional experiments were conducted to determine the Faradaic efficiency and to study longer-term stability. A list of the catalysts for which these additional studies were performed is shown in Table 2. As a secondary screen of catalyst stability, we conducted longer term stability studies on particularly active catalysts. These studies consisted of holding the electrode at a constant magnitude 10 mA cm^{-2} current density for 24 h and measuring the change in overpotential during this time. The overpotentials necessary to achieve 10 mA cm^{-2} current density at time = 24 h ($\eta_{t=24h}$) averaged from at least 3 independent experiments are summarized for select catalysts in Table 2.

In addition, the Faradaic efficiencies, ε, of OER and HER catalysts were determined by quantifying the amount of dissolved O$_2$ or H$_2$ generated during an electrolysis using O$_2$ and H$_2$ probes and dividing that by the amount of O$_2$ or H$_2$ expected based on the charge passed during that electrolysis. Representative Faradaic efficiency measurements for HER at NiMo-(a) in 1 M H$_2$SO$_4$ and 1 M NaOH, and OER at Co-(b)
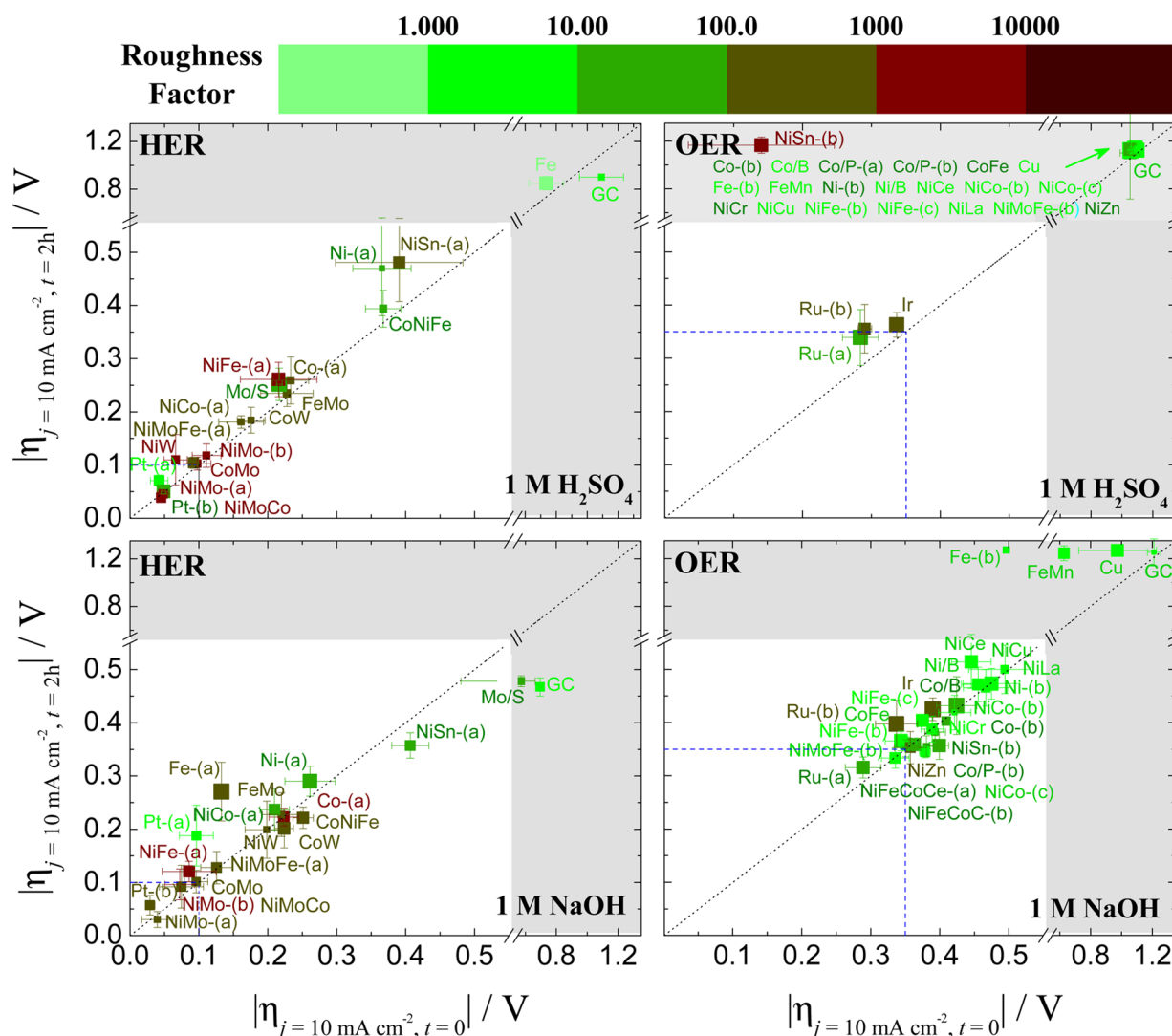
Figure 2. Plots of catalytic activity, stability, and electrochemically active surface area for HER (left) and OER (right) electrocatalysts in acidic (top) and alkaline (bottom) solutions. The x-axis is the overpotential required to achieve 10 mA cm^{-2} per geometric area at time $t = 0$. The y-axis is the overpotential required to achieve 10 mA cm^{-2} per geometric area at time $t = 2$ h. The diagonal dashed line is the expected response for a stable catalyst that does not change in activity during 2 h constant polarization. The color of the each point represents the roughness factor of the catalyst with a bin size of 1 order of magnitude with light green representing RF = 1, and dark red representing RF > 10^4. The size of each point is inversely proportional to the standard deviation in the ECSA measurements. The region of interest for benchmarking is the unshaded white region of the plot where the overpotential required to achieve 10 mA cm^{-2} per geometric area at time $t = 0$ and $t = 2$ h is less than 0.55 V. There is a break and change in scale in both axes at overpotentials >0.55 V, and the corresponding region of the plot is shown in gray. Catalysts whose activity and stability measurements fall inside this gray area are outside the region of interest for benchmarking, but their activity and stability measurements are included for completeness. The blue boxed regions are the target regions for HER and OER catalysis under the given conditions.

in 1 M NaOH are shown in Figures S10−S12. The measured ε for selected OER and HER catalysts measured at a disk current of 10 mA cm^{-2} are shown in Table 2. In general, each catalyst produced H$_2$ or O$_2$ with near-unity Faradaic efficiency.

One exception is the Co/P-(b) OER catalyst. The as-deposited Co/P-(b) catalyst operates with a Faradaic efficiency of $\varepsilon \sim 0.7$ at 10 mA cm^{-2} in 1 M NaOH. However, an examination of 24 h controlled-potential electrolysis experiments shows an increase in catalytic activity over the course of the first ~16 h of OER performance (Figure S13). This suggests that some of the initial current in the OER experiments is going toward catalyst activation instead of water oxidation, which could account for the lower-than-unity Faradaic efficiency of the as-deposited material. Faradaic efficiency measurements on the material subsequent to 24 h

OER measurements showed near-unity Faradaic efficiency (Figure S14), which supports this hypothesis.

Comparison of HER Catalyst Performance. In the case of HER, the polished polycrystalline Pt-(a) electrode and platinized Pt-(b) electrode show the highest activity in acidic solution, achieving 10 mA cm^{-2} at $\eta_{t=0} \sim -0.04$ in agreement with previous studies.[72−74] However, the electrodeposited NiMo-(a) and NiMoCo, show similar geometric activity in acid to that of Pt-(a) and Pt-(b), achieving 10 mA cm^{-2} at $\eta_{t=0}$ = −0.045 ± 0.004 V and $\eta_{t=0}$ = −0.05 ± 0.01 V, respectively, with no loss of activity after 2 h of constant polarization. It is important to note that the ECSA determined for electro-deposited NiMo-(a) and NiMoCo catalysts is over 100× larger than that of Pt-(a) and over 10× larger than that of Pt-(b), and thus the two electrodeposits have significantly lower specific
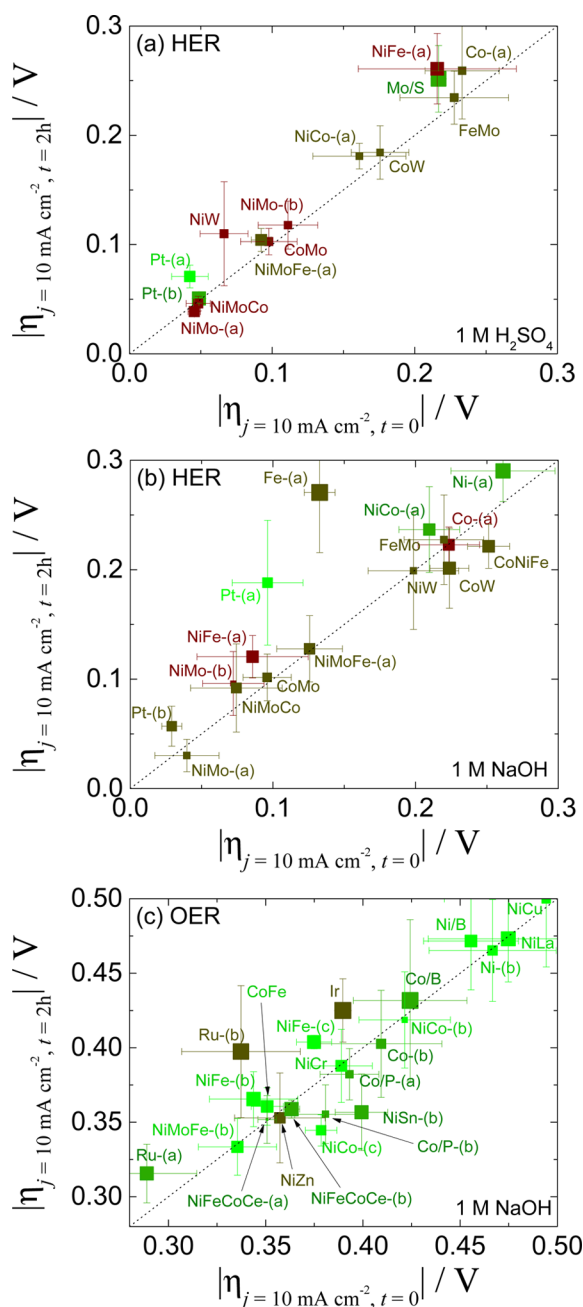
Figure 3. Zoomed in region for (a) acidic HER, (b) alkaline HER, and (c) alkaline OER from Figure 2. The x-axis is the overpotential required to achieve 10 mA cm^{-2} per geometric area at time $t = 0$. The y-axis is the overpotential required to achieve 10 mA cm^{-2} per geometric area at time $t = 2$ h. The diagonal dashed line is the expected response for a stable catalyst. The color of the each point represents the roughness factor of the catalyst with a bin size of 1 order of magnitude as shown in Figure 2. The size of each point is inversely proportional to the standard deviation in the ECSA measurements.

activity. Other catalysts that show high activity and 2 h stability in 1 M H$_2$SO$_4$ with $\eta_{t=0} \sim \eta_{t=2h} \leq 0.15$ V include CoMo, NiMoCo, NiMo-(b), NiMoFe-(a), and NiW-(a).

Note that the activity of Pt-(a) and Pt-(b) in 1 M H$_2$SO$_4$ as measured by rotating disk voltammetry is lower than the expected *true* activity of Pt.[73,75−77] This is because Pt is sufficiently active such that the HER activity of Pt in an RDE measurement is limited by a hydrogen diffusion overpotential

rather than the intrinsic kinetics of the catalytic reaction.[73,77,78] The existence of this diffusion overpotential also explains why planar Pt-(a) shows roughly equivalent activity per geometric area to that of platinized Pt-(b) in 1 M H$_2$SO$_4$. While RDE measurements cannot be used to establish the *true* kinetically limited HER activity of Pt, they are still likely an appropriate approximation for the mass-transport limited *operating* activity relevant to an integrated device. This is because in a typical 2-electrode integrated water splitting cell, mass transport is controlled either by turbulent mixing via bubble formation or rapid stirring, or by controlled flow in a flow-cell geometry.[79−83] In such setups, similar diffusion overpotentials to those in the RDE measurements will limit Pt activity.

When investigating HER in 1 M NaOH, Pt-(a) shows lower activity compared to its activity in 1 M H$_2$SO$_4$, achieving 10 mA cm^{-2} at $\eta_{t=0} \sim -0.10 \pm 0.02$ V. The lower HER activity of Pt in alkaline solution as compared to acidic solution is previously reported,[78,84,85] although no consensus exists as to the reason for this decreased activity and the broader topic of the effect of pH on noble-metal catalysis is currently a topic of vigorous scientific discussion.[86,87] Note that higher-surface area platinized Pt-(b) operates with higher activity than planar Pt-(a) as one would expect, operating with at 10 mA cm^{-2} current density at $\eta_{t=0} \sim -0.04$ in 1 M NaOH. The activity per geometric area of Pt-(b) in 1 M NaOH is equivalent to the activity of Pt-(a) and Pt-(b) in 1 M H$_2$SO$_4$, although the specific activity of Pt-(b) in 1 M NaOH is roughly 5−20× lower than that of Pt-(a) or Pt-(b) in acidic solution.

Pt-(a) also shows a much larger decrease in activity during 2 h polarization measurements in 1 M NaOH compared to 1 M H$_2$SO$_4$, with the overpotential necessary to achieve 10 mA cm^{-2} increasing in magnitude by ~0.1 V to $\eta_{t=2h} = -0.19 \pm 0.06$ V in 1 M NaOH after 2 h of constant polarization, compared to an increase in magnitude of only 0.03 V from ~ -0.04 to -0.07 V in 1 M H$_2$SO$_4$. Note that this loss of activity is likely at least partially due to surface poisoning from leached contaminants from the glass cells used in the measurements.[88,89] By comparison, higher surface area platinized Pt-(b) showed greater stability as one would expect: leached contiments will poison a smaller fraction of the high-surface area Pt, leading to increased comparative stability to planar Pt.

In comparison to Pt-(a) and Pt-(b), several materials show similar activity in 1 M NaOH, including NiMo-(a), NiMoCo, CoMo, NiMo-(b), NiFe-(a), and NiMoFe-(a). Again, each of these materials have 1−3 orders of magnitude higher surface area than Pt-(a) and Pt-(b), and this increased surface area likely accounts at least partially for the relatively greater geometric activity of these materials.

Longer term, 24 h stability measurements were conducted in 1 M H$_2$SO$_4$ and 1 M NaOH for 5 HER catalysts as summarized in Table 2. In general, each material investigated for the 24 h stability test showed reasonable stability under constant polarization with operating overpotentials at -10 mA cm^{-2}, changing by less than 0.06 V. One exception is NiW which shows a decrease in HER activity in 1 M H$_2$SO$_4$ as evidenced by the >0.2 V increase in the magnitude overpotential at 10 mA cm^{-2} over the course of 24 h.

Comparison of OER Catalyst Performance. A few key observations become apparent from an examination of the OER data in Figure 2. The most striking result is that none of the non-noble metal catalysts investigated were stable under OER conditions in 1 M H$_2$SO$_4$. This is not surprising given the general thermodynamic instability of many transition metal

oxides such as cobalt- and nickel-oxides under oxidative conditions in strong acid as shown in Pourbaix diagrams.[90,91]

Another noteworthy observation is that under alkaline conditions, most catalysts operate with roughly equivalent activity for OER, achieving 10 mA cm^{-2} current densities at overpotentials of $\eta_{t=0} = 0.35-0.50$ V. This observation is similar to the trend we previously observed in our preliminary benchmarking study for OER,[26] albeit now with a larger sample set, and may suggest common mechanistic limitations. It has been postulated that oxide-based OER catalysts operate via a common mechanism that includes the formation of a surface hydroxide OH* intermediate which is oxidized by two electrons to a surface hydroperoxy OOH* intermediate.[92-95] DFT calculations suggest that the difference in binding energies of these two intermediates is similar regardless of the metal oxide surface to which the intermediates are coordinated.[95] This "scaling relation" implies that there is a minimum "thermodynamic overpotential" of ~0.4 V for OER at planar metal-oxide surfaces calculated assuming only thermodynamic considerations.[92,95] This hypothesis is quantitatively consistent with the activity measurements reported in this study: all non-noble metal catalysts evaluated operate at $j = 10$ mA cm^{-2} with overpotentials $\eta_{t=0} \geq 0.30$ V in 1 M NaOH.

Although many of these catalysts are roughly equivalent in activity, one can still identify a few catalysts with relatively high activity and stability compared to the others. Upon examination of the zoomed-in region of interest for OER in 1 M NaOH shown in Figure 3, one can quickly identify NiMoFe-(b) as the only non-noble metal catalyst evaluated that operates at 10 mA cm^{-2} with an overpotential $\eta_{t=0} \sim \eta_{t=2h} < 0.35$ V. Although Ir, Ru-(a), and Ru-(b) have equivalent or higher activity per geometric area than NiMoFe-(b), they have lower specific activity due to their relatively higher surface areas. Additional catalysts that operate at 10 mA cm^{-2} with overpotentials of 0.35 V $< \eta_{t=0} \sim \eta_{t=2h} < 0.39$ V include Co/P-(b), CoFe, NiCo-(c), NiFe-(b), NiFeCoCe-(a), NiFeCoCe-(b), NiSn-(b), and NiZn. An additional tier of catalytic materials that operate with overpotentials of 0.40 V $< \eta_{t=0} \sim \eta_{t=2h} < 0.45$ V includes Co-(b), Co/B, Co/P-(a), NiCo-(b), and NiCr.

Longer term, 24 h stability measurements were conducted in 1 M NaOH for 12 OER catalysts as summarized in Table 1. Of the OER catalysts investigated, Co/P-(a), Co/P-(b), CoFe, NiCo-(c), NiFe-(b), NiMoFe-(b), NiZn-(b), and Ru-(a) showed excellent longer-term stability as the overpotential required to maintain a current density of 10 mA cm^{-2} either held constant or even decreased over the 24 h. Both Co-(b) and NiCr showed variable 24 h stability in multiple experiments, with roughly half the samples prepared exhibiting 24 h stability and half suffering a catastrophic loss of activity after ca. 18−22 h (Figures S16−S17). This suggests that these two materials would likely be unstable to more rigorous stability testing. Ni-(b) and NiCo-(b) lost all catalytic activity and showed background GC activity after 24 h of constant polarization.

Stability of NiMo in H$_2$SO$_4$ for HER. The 24 h stability of NiMo-(a) and NiMo-(b) are particularly interesting considering the generally accepted acid instability of NiMo-based catalysts.[96,97] Corrosion studies of pure NiMo alloys with >20% Mo composition report corrosion rates in 10% HCl at 70 °C of ~300 mg dm^{-2} day^{-1} (mdd), although this drops to ~50 mdd in deaerated solutions at 70 °C and to rates below the detectable limits in 10% HCl solutions at 25 °C.[98] However, the reported corrosion rate for NiMo materials with 27% Mo

content electrodeposited from solutions containing citrate anions onto carbon electrodes and measured in 1 M H$_2$SO$_4$ at 60 °C is 5.8×10^3 mdd.[99]

Of the few reports that examine the HER activity of NiMo in acid,[47,97,100−107] most do not address the stability of the material under HER conditions. However, NiMo nanoparticles have been reported to be unstable in acid under HER conditions, increasing in overpotential by ~0.04−0.05 V after ~20 h of constant polarization at −20 mA cm^{-2} in 1 M H$_2$SO$_4$,[106] and fully degrading after 2000 cycles between −0.3 to 0.9 V vs RHE in 0.1 M HClO$_4$.[97] NiMo-nitride nanosheets have been reported to have enhanced stability over the course of 2000 cycles between −0.3 to 0.9 V vs RHE in 0.1 M HClO$_4$.[97]

Additional stability measurements were conducted to test the stability of the NiMo-(a) electrodeposit under HER conditions by measuring multiple cyclic voltammograms between −0.1 to 0.1 V vs RHE for 10 000 cycles at 50 mV s^{-1} scan rate in 1 M H$_2$SO$_4$. This range was chosen such that the positive limit is slightly positive of the thermodynamic H$^+$/H$_2$ potential and the negative limit is sufficiently negative to achieve initial maximum current densities on the order of −100 mA cm^{-2}. Every 50th voltammogram was conducted at a scan rate of 10 mV s^{-1} followed by a 30s chronopotentiometric step at −10 mA cm^{-2} current density. The overpotential measurements at −10 mA cm^{-2} current density after 500 cycle intervals for NiMo-(a) for 10 independent experiments are shown in Figure S18. There was a modest increase in the magnitude of the overpotential by ~0.050 V over the course of the 10 000 cycles to $\eta_{10000cycles} = -0.087 \pm 0.046$ V. A comparison of the average overpotential measurements at 10 mA cm^{-2} for the 10 000 cycle experiments and the 24 h constant polarization experiments for NiMo-(a) are shown in Figure 4. The result from the cycling experiment is qualitatively and quantitatively different than the 24 h constant polarization measurements, which showed a very modest enhancement of catalytic activity after cathodic polarization. A longer-term stability test in which the potential was cycled using the same procedure but for >20 000 cycles showed an increase in the magnitude of the overpotential by ~0.15 V over the course of 20 000 cycles to $\eta_{20000cycles} = -0.20 \pm 0.12$ V, and by ≥0.4 V after 30 000 cycles (Figure S19). This suggests that the shorter-term, 24 h stability studies are insufficient probes of long-term catalyst stability. For comparison, NiMo-(a) shows enhanced catalyst stability in 1 M NaOH, increasing in magnitude overpotential by <0.02 V over the course of 40 000 cycles (Figure S20).

These stability results for NiMo-(a) highlight the need for further long-term stability and accelerated durability investigations in acid of NiMo and other HER materials to determine their feasibility for incorporation into integrated solar-fuel devices. Such protocols would allow for the stability of catalysts such as NiMo-(a) to be directly compared to other reported acid-stable catalysts such as various Ni/P,[103,108] Co/P,[109] and Mo/S materials.[43,60,110]

■ CONCLUSIONS

A benchmarking protocol was used to evaluate the performance of 16 HER and 23 OER catalysts comprised of earth-abundant materials in 1 M NaOH and 1 M H$_2$SO$_4$ at current densities relevant to a 10% efficient solar water splitting device under 1 sun illumination. Each material was deposited onto a glassy carbon substrate, and the activity, stability, and electrochemically active surface area of each material was measured. These
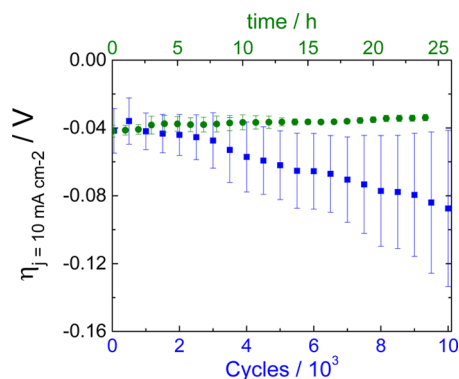
Figure 4. Extended stability studies for NiMo-(a) in 1 M H_2SO_4. The green circles are the average measured overpotentials during 24 h constant current electrolysis measurements plotted vs the polarization time on the top x-axis. The blue squares are the average measured overpotentials from intermittent 30 s chronopotentiometric steps during 10 000 cycle experiments plotted vs the number of cycles on the bottom x-axis. Note that the 10 000 cycle experiment lasts ca. 25 h, and the top axis also reflects the time point in the cycling measurement at which the operating overpotential was measured. The 24 h measurements were averaged from three separate experiments, and the 10 000 cycle measurements were averaged from ten separate experiments (Figure S18). The error bars show the standard deviation of the measurements. The catalyst remains active during both stability studies, with the magnitude of the overpotential at 10 mA cm^{-2} decreasing by ~0.010 V to $\eta_{t=24h} = -0.034 \pm 0.006$ V during 24 h constant polarization and increasing in magnitude by ~0.050 V to $\eta_{10000cycles} = -0.087 \pm 0.046$ over the course of 10 000 potential cycles between -0.1 to 0.1 V vs RHE.

measurements are summarized in a graphical representation (Figure 2) for easy comparison of catalytic data. A Pt disk electrode and a platinized Pt electrode were also investigated for comparison for HER, and a sputtered Ir catalyst and 2 different deposited Ru catalysts were investigated for comparison for OER.

In the case of OER, most catalysts investigated were oxidatively unstable in acidic conditions. Only Ir, Ru-(a), and Ru-(b) showed appreciable activity and stability in 1 M H_2SO_4, maintaining 10 mA cm^{-2} current density at $\eta \leq 0.36$ V after 2 h constant polarization. This suggests that there is a need to develop non-noble metal OER catalysts that are oxidatively stable in acid if precious metals are to be avoided in solar water-splitting devices operating in acidic solution. In 1 M NaOH, most OER catalysts investigated in this study showed fairly similar activity to one another, achieving 10 mA cm^{-2} current densities at overpotentials between 0.3 V $\leq \eta \leq$ 0.5 V. Of particular note is the NiMoFe-(b) catalyst that showed comparable activity per geometric area and higher specific activity than the various Ir and Ru catalysts investigated, as well as promising 24 h stability under constant polarization. All non-noble metal catalysts investigated required $\eta > 0.3$ V driving force to achieve current densities of 10 mA cm^{-2}.

Several HER catalysts show high activity and stability in 1 M H_2SO_4 and/or 1 M NaOH, achieving -10 mA cm^{-2} with magnitude overpotentials $|\eta_{t=0}| \sim |\eta_{t=2h}| \leq$ ~0.1 V. The stability of the NiMo-based catalysts was particularly surprising given the reported acid instability of NiMo nanoparticles.[97,106] Potential cycling experiments between 0.1 to -0.1 V vs RHE were conducted to further test the long-term stability of NiMo-(a), and the magnitude overpotential necessary for the catalyst to achieve 10 mA cm^{-2} increased by <0.05 V after over 10 000

cycles. The NiMo-(a) catalyst shows the same activity and stability as many recently reported acid-stable HER catalysts.[43,60,103,108−110] However, the NiMo-(a) catalyst degraded in catalytic activity over time, eventually operating with >0.4 V magnitude overpotential at -10 mA cm^{-2} after 30 000 cycles. This result highlights the need for the development of an accelerated durability protocol, perhaps similar in concept to the one proposed for fuel-cell catalyst testing,[111−116] to better evaluate catalyst stability under relevant device conditions.

The benchmarking protocol reported here allows for rapid, preliminary evaluation of catalyst performance. However, further in-depth catalyst testing for promising materials is necessary to better evaluate catalyst performance under specific operating conditions once they are defined. This may include the establishment of accelerated life testing to better probe the long-term stability of various OER and HER materials and the study of light absorbing properties of catalyst materials under operating conditions. It is important to consider that the benchmarking conditions and figures of merit reported here are specific to an integrated solar water-splitting device operating in strongly acidic or alkaline conditions under 1 sun illumination; these conditions may be different than those required to evaluate catalyst performance for other devices or operating conditions, such as PEM and alkaline water electrolyzers or integrated water-splitting cells under multiple-sun illumination.

■ ASSOCIATED CONTENT

⑤ Supporting Information

List of chemicals used in electrode preparations and electrocatalytic measurements; pictures of electrolysis cell used for Faradaic efficiency measurements; preparations of electrodeposited catalyst materials; data tables summarizing activity, stability, surface area, and specific activity of each catalyst investigated; representative scan-rate dependence of non-Faradaic cyclic voltammograms for determination of double-layer capacitance for NiMo-(a) and Co-(b); representative rotating disk voltammograms, chronopotentiometric step data and chronoamperometric steps data for NiMo-(a) and Co-(b); representative Faradaic efficiency measurements for NiMo-(a) and Co-(b); representative 24 h OER stability measurements and Faradaic efficiency measurements for Co/P-(b) in 1 M NaOH; representative 24 h OER stability measurements for Ru-(a), Co-(b) and NiCr in 1 M NaOH; potential cyclic experiments for accelerated durability testing of NiMo-(a) in 1 M H_2SO_4 and 1 M NaOH; X-ray photoelectron spectra of each material evaluated. This material is available free of charge via the Internet at http://pubs.acs.org.

■ AUTHOR INFORMATION

Corresponding Author

*benchmarking@solarfuelshub.org

Notes

The authors declare no competing financial interest.

■ ACKNOWLEDGMENTS

■ REFERENCES

(1) Grätzel, M. *Acc. Chem. Res.* **1981**, *14*, 376−384.

(2) Koelle, U. *New J. Chem.* **1992**, *16*, 157−169.

(3) Bard, A. J.; Fox, M. A. *Acc. Chem. Res.* **1995**, *28*, 141−145.

(4) Turner, J. A. *Science* **2004**, *305*, 972−974.

(5) Lewis, N. S.; Nocera, D. G. *Proc. Natl. Acad. Sci. U. S. A.* **2006**, *103*, 15729−15735.

(6) Lewis, N. S. *Science* **2007**, *315*, 798−801.

(7) Crabtree, G. W.; Dresselhaus, M. S. *MRS Bull.* **2008**, *33*, 421−428.

(8) Gray, H. B. *Nat. Chem.* **2009**, *1*, 7.

(9) Walter, M. G.; Warren, E. L.; McKone, J. R.; Boettcher, S. W.; Mi, Q.; Santori, E. A.; Lewis, N. S. *Chem. Rev.* **2010**, *110*, 6446−6473.

(10) Cook, T. R.; Dogutan, D. K.; Reece, S. Y.; Surendranath, Y.; Teets, T. S.; Nocera, D. G. *Chem. Rev.* **2010**, *110*, 6474−6502.

(11) Trasatti, S. In *Advances in Electrochemical Science and Engineering*; Wiley-VCH Verlag GmbH: Weinheim, 1992; Vol. 2, pp 1−85.

(12) Trasatti, S. In *Interfacial Electrochemistry*; Wieckowski, A., Ed.; Marcel Dekker, Inc.: New York, 1999; pp 769−792.

(13) Matsumoto, Y.; Sato, E. *Mater. Chem. Phys.* **1986**, *14*, 397−426.

(14) Chen, W.-F.; Muckerman, J. T.; Fujita, E. *Chem. Commun.* **2013**, *49*, 8896−8909.

(15) Jakšić, M. M. *Electrochim. Acta* **1984**, *29*, 1539−1550.

(16) Jaramillo, T. F.; Ivanovskaya, A.; McFarland, E. W. *J. Comb. Chem.* **2001**, *4*, 17−22.

(17) Chen, G.; Delafuente, D. A.; Sarangapani, S.; Mallouk, T. E. *Catal. Today* **2001**, *67*, 341−355.

(18) Gerken, J. B.; Chen, J. Y. C.; Massé, R. C.; Powell, A. B.; Stahl, S. S. *Angew. Chem., Int. Ed.* **2012**, *51*, 6676−6680.

(19) Liu, X.; Shen, Y.; Yang, R.; Zou, S.; Ji, X.; Shi, L.; Zhang, Y.; Liu, D.; Xiao, L.; Zheng, X.; Li, S.; Fan, J.; Stucky, G. D. *Nano Lett.* **2012**, *12*, 5733−5739.

(20) Gregoire, J. M.; Xiang, C.; Mitrovic, S.; Liu, X.; Marcin, M.; Cornell, E. W.; Fan, J.; Jin, J. *J. Electrochem. Soc.* **2013**, *160*, F337−F342.

(21) Seley, D.; Ayers, K.; Parkinson, B. A. *ACS Comb. Sci.* **2013**, *15*, 82−89.

(22) Berglund, S. P.; Lee, H. C.; Nunez, P. D.; Bard, A. J.; Mullins, C. B. *Phys. Chem. Chem. Phys.* **2013**, *15*, 4554−4565.

(23) Haber, J. A.; Cai, Y.; Jung, S.; Xiang, C.; Mitrovic, S.; Jin, J.; Bell, A. T.; Gregoire, J. M. *Energy Environ. Sci.* **2014**, *7*, 682−688.

(24) Nørskov, J. K.; Bligaard, T.; Logadottir, A.; Bahn, S.; Hansen, L. B.; Bollinger, M.; Bengaard, H.; Hammer, B.; Sljivancanin, Z.; Mavrikakis, M.; Xu, Y.; Dahl, S.; Jacobsen, C. J. H. *J. Catal.* **2002**, *209*, 275−278.

(25) Nørskov, J. K.; Abild-Pedersen, F.; Studt, F.; Bligaard, T. *Proc. Natl. Acad. Sci. U. S. A.* **2011**, *108*, 937−943.

(26) McCrory, C. C. L.; Jung, S.; Peters, J. C.; Jaramillo, T. F. *J. Am. Chem. Soc.* **2013**, *135*, 16977−16987.

(27) Weber, M. F.; Dignam, M. J. *J. Electrochem. Soc.* **1984**, *131*, 1258−1265.

(28) Gorlin, Y.; Jaramillo, T. F. *J. Am. Chem. Soc.* **2010**, *132*, 13612−13614.

(29) Liaudet, E.; Battaglini, F.; Calvo, E. J. *J. Electroanal. Chem.* **1990**, *293*, 55−68.

(30) *NIST X-Ray Photoelectron Spectroscopy Database*, Version 4.1; National Institute of Standards and Technology: Gaithersburg, MD, 2012; http://srdata.nist.gov/xps/.

(31) Wagner, C. D.; Riggs, W. M.; Davis, L. E.; Moulder, J. F. *Handbook of X-ray Photoelectron Spectroscopy*, 1st ed.; Physical Electronics Division, Perkin-Elmer Corp.: Eden Prairie, MN, 1979.

(32) Moulder, J. F.; Stickle, W. F.; Sobol, P. E.; Bomben, K. *Handbook of X-Ray Photoelectron Spectroscopy*, 2nd ed.; Physical Electronics Division, Perkin Elmer Corp.: Eden Prairie, MN, 1992.

(33) Spurgeon, J. M.; Velazquez, J. M.; McDowell, M. T. *Phys. Chem. Chem. Phys.* **2014**, *16*, 3623−3631.

(34) Savadogo, O.; Lavoie, H. *Int. J. Hydrogen Energy* **1992**, *17*, 473−477.

(35) Merrill, M. D.; Dougherty, R. C. *J. Phys. Chem. C* **2008**, *112*, 3655−3666.

(36) Fan, C.; Piron, D. L.; Sleb, A.; Paradis, P. *J. Electrochem. Soc.* **1994**, *141*, 382−387.

(37) Surendranath, Y.; Dincă, M.; Nocera, D. G. *J. Am. Chem. Soc.* **2009**, *131*, 2615−2620.

(38) Jafarian, M.; Azizi, O.; Gobal, F.; Mahjani, M. G. *Int. J. Hydrogen Energy* **2007**, *32*, 1686−1693.

(39) Kanan, M. W.; Nocera, D. G. *Science* **2008**, *321*, 1072−1075.

(40) Surówka, J.; Budniok, A.; Bzowski, B.; Warczewski, J. *Thin Solid Films* **1997**, *307*, 233−239.

(41) Solmaz, R.; Kardaş, G. *Electrochim. Acta* **2009**, *54*, 3726−3734.

(42) Elezović, N. R.; Jović, V. D.; Krstajić, N. V. *Electrochim. Acta* **2005**, *50*, 5594−5601.

(43) Merki, D.; Fierro, S.; Vrubel, H.; Hu, X. *Chem. Sci.* **2011**, *2*, 1262−1267.

(44) Merki, D.; Vrubel, H.; Rovelli, L.; Fierro, S.; Hu, X. *Chem. Sci.* **2012**, *3*, 2515−2525.

(45) Raj, I. A.; Vasu, K. I. *J. Appl. Electrochem.* **1990**, *20*, 32−38.

(46) Corrigan, D. A.; Bendert, R. M. *J. Electrochem. Soc.* **1989**, *136*, 723−728.

(47) Navarro-Flores, E.; Chong, Z.; Omanovic, S. *J. Mol. Catal. A: Chem.* **2005**, *226*, 179−197.

(48) Dincă, M.; Surendranath, Y.; Nocera, D. G. *Proc. Natl. Acad. Sci. U. S. A.* **2010**, *107*, 10337−10341.

(49) Krstajić, N. V.; Jović, V. D.; Gajić-Krstajić, L.; Jović, B. M.; Antozzi, A. L.; Martelli, G. N. *Int. J. Hydrogen Energy* **2008**, *33*, 3676−3687.

(50) Fan, C.; Piron, D. L.; Paradis, P. *Electrochim. Acta* **1994**, *39*, 2715−2722.

(51) Raj, I. A.; Vasu, K. I. *J. Appl. Electrochem.* **1992**, *22*, 471−477.

(52) Ho, J. C. K.; Piron, D. L. *J. Appl. Electrochem.* **1996**, *26*, 515−521.

(53) Yamashita, H.; Yamamura, T.; Yoshimoto, K. *J. Electrochem. Soc.* **1993**, *140*, 2238−2243.

(54) Li, X.; Walsh, F. C.; Pletcher, D. *Phys. Chem. Chem. Phys.* **2011**, *13*, 1162−1167.

(55) Walton, D. J.; Burke, L. D.; Murphy, M. M. *Electrochim. Acta* **1996**, *41*, 2747−2751.

(56) Corrigan, D. A. *J. Electrochem. Soc.* **1987**, *134*, 377−384.

(57) Jayalakshmi, M.; Kim, W. Y.; Jung, K. D.; Joo, O. S. *Int. J. Electrochem. Sci.* **2008**, *3*, 908.

(58) Santos, M. B. F.; da Silva, E. P.; Andrade, R., Jr.; Dias, J. A. F. *Electrochim. Acta* **1992**, *37*, 29−32.

(59) Tsuji, E.; Imanishi, A.; Fukui, K.-i.; Nakato, Y. *Electrochim. Acta* **2011**, *56*, 2009−2016.

(60) Benck, J. D.; Chen, Z.; Kuritzky, L. Y.; Forman, A. J.; Jaramillo, T. F. *ACS Catal.* **2012**, *2*, 1916−1923.

(61) Weisenberger, S.; Schumpe, A. *AIChE J.* **1996**, *42*, 298−300.

(62) Battino, R. *J. Phys. Chem. Ref. Data* **1983**, *12*, 163−178.

(63) Linke, W. F. *Solubilities: Inorganic and Metal-Organic Compounds*, 4th ed.; American Chemical Society: Washington, D.C., 1965; Vol. 2, pp 1229−1230.

(64) Klauber, C.; Smart, R. S. C. In *Surface Analysis Methods in Materials Science*, 2nd ed.; O'Conner, D. J., Sexton, B. A., Smart, R. S. C., Eds.; Springer-Verlag: Berlin, 2003; pp 3−65.

(65) Chusuei, C. C.; Goodman, D. W. In *Encyclopedia of Physical Science and Technology*, 3rd ed.; Robert, A. M., Ed.; Academic Press: New York, 2003; pp 921−938.

(66) Trasatti, S.; Petrii, O. A. *Pure Appl. Chem.* **1991**, *63*, 711−734.

(67) Bockris, J. O. M.; Srinivasan, S. *J. Electroanal. Chem.* **1966**, *11*, 350−389.

(68) Boggio, R.; Carugati, A.; Trasatti, S. *J. Appl. Electrochem.* **1987**, *17*, 828−840.

(69) Weber, M. F.; Dignam, M. J. *Int. J. Hydrogen Energy* **1986**, *11*, 225−232.

(70) Seitz, L. C.; Chen, Z.; Forman, A. J.; Pinaud, B. A.; Benck, J. D.; Jaramillo, T. F. *ChemSusChem* **2014**, *7*, 1372−1385.

(71) Stoerzinger, K. A.; Qiao, L.; Biegalski, M. D.; Shao-Horn, Y. *J. Phys. Chem. Lett.* **2014**, *5*, 1636−1641.

(72) Schuldiner, S.; Hoare, J. P. *Can. J. Chem.* **1959**, *37*, 228−237.

(73) Neyerlin, K. C.; Gu, W.; Jorne, J.; Gasteiger, H. A. *J. Electrochem. Soc.* **2007**, *154*, B631−B635.

(74) Barber, J.; Morin, S.; Conway, B. E. *J. Electroanal. Chem.* **1998**, *446*, 125−138.

(75) Danilovic, N.; subbaraman, R.; Strmcnik, D.; Stamenkovic, V. R.; Markovic, N. M. *J. Serb. Chem. Soc.* **2013**, *78*, 2007−2015.

(76) Rheinländer, P. J.; Herranz, J.; Durst, J.; Gasteiger, H. A. *J. Electrochem. Soc.* **2014**, *161*, F1448−F1457.

(77) Durst, J.; Simon, C.; Hasché, F.; Gasteiger, H. A. *J. Electrochem. Soc.* **2015**, *162*, F190−F203.

(78) Sheng, W.; Gasteiger, H. A.; Shao-Horn, Y. *J. Electrochem. Soc.* **2010**, *157*, B1529−B1536.

(79) Fujishima, A.; Honda, K. *Nature* **1972**, *238*, 37−38.

(80) Khaselev, O.; Turner, J. A. *Science* **1998**, *280*, 425−427.

(81) Reece, S. Y.; Hamel, J. A.; Sung, K.; Jarvi, T. D.; Esswein, A. J.; Pijpers, J. J. H.; Nocera, D. G. *Science* **2011**, *334*, 645−648.

(82) Han, L.; Abdi, F. F.; van de Krol, R.; Liu, R.; Huang, Z.; Lewerenz, H.-J.; Dam, B.; Zeman, M.; Smets, A. H. M. *ChemSusChem* **2014**, *7*, 2832−2838.

(83) Jin, J.; Walczak, K.; Singh, M. R.; Karp, C.; Lewis, N. S.; Xiang, C. *Energy Environ. Sci.* **2014**, *7*, 3371−3380.

(84) Markovica, N. M.; Sarraf, S. T.; Gasteiger, H. A.; Ross, P. N. *J. Chem. Soc., Faraday Trans.* **1996**, *92*, 3719−3725.

(85) Conway, B. E.; Bai, L. *J. Electroanal. Chem.* **1986**, *198*, 149−175.

(86) Strmcnik, D.; Uchimura, M.; Wang, C.; Subbaraman, R.; Danilovic, N.; van der, V.; Paulikas, A. P.; Stamenkovic, V. R.; Markovic, N. M. *Nat. Chem.* **2013**, *5*, 300−306.

(87) Durst, J.; Siebel, A.; Simon, C.; Hasche, F.; Herranz, J.; Gasteiger, H. A. *Energy Environ. Sci.* **2014**, *7*, 2255−2260.

(88) Mayrhofer, K. J. J.; Wiberg, G. K. H.; Arenz, M. *J. Electrochem. Soc.* **2008**, *155*, P1−P5.

(89) Mayrhofer, K. J. J.; Crampton, A. S.; Wiberg, G. K. H.; Arenz, M. *J. Electrochem. Soc.* **2008**, *155*, P78−P81.

(90) Pourbaix, M. *Atlas of Electrochemical Equilibria in Aqueous Solution*; Pergamon Press: Oxford, 1966.

(91) Minguzzi, A.; Fan, F.-R. F.; Vertova, A.; Rondinini, S.; Bard, A. *J. Chem. Sci.* **2012**, *3*, 217−229.

(92) Man, I. C.; Su, H.-Y.; Calle-Vallejo, F.; Hansen, H. A.; Martínez, J. I.; Inoglu, N. G.; Kitchin, J.; Jaramillo, T. F.; Nørskov, J. K.; Rossmeisl, J. *ChemCatChem* **2011**, *3*, 1159−1165.

(93) Rossmeisl, J.; Logadottir, A.; Nørskov, J. K. *Chem. Phys.* **2005**, *319*, 178−184.

(94) Rossmeisl, J.; Qu, Z. W.; Zhu, H.; Kroes, G. J.; Nørskov, J. K. *J. Electroanal. Chem.* **2007**, *607*, 83−89.

(95) Koper, M. T. M. *J. Electroanal. Chem.* **2011**, *660*, 254−260.

(96) McKone, J. R.; Marinescu, S. C.; Brunschwig, B. S.; Winkler, J. R.; Gray, H. B. *Chem. Sci.* **2014**, *5*, 865−878.

(97) Chen, W.-F.; Sasaki, K.; Ma, C.; Frenkel, A. I.; Marinkovic, N.; Muckerman, J. T.; Zhu, Y.; Adzic, R. R. *Angew. Chem., Int. Ed.* **2012**, *51*, 6131−6135.

(98) Uhlig, H. H.; Bond, P.; Feller, H. *J. Electrochem. Soc.* **1963**, *110*, 650−653.

(99) Stepanova, L. I.; Purovskaya, O. G. *Met. Finish.* **1998**, *96*, 50−53.

(100) Damian, A.; Omanovic, S. *J. Power Sources* **2006**, *158*, 464−476.

(101) Highfield, J. G.; Oguro, K.; Grushko, B. *Electrochim. Acta* **2001**, *47*, 465−481.

(102) Highfield, J. G.; Claude, E.; Oguro, K. *Electrochim. Acta* **1999**, *44*, 2805−2814.

(103) Lu, G.; Evans, P.; Zangari, G. *J. Electrochem. Soc.* **2003**, *150*, A551−A557.

(104) Martinez, S.; Metikoš-Huković, M.; Valek, L. *J. Mol. Catal. A: Chem.* **2006**, *245*, 114−121.

(105) Aaboubi, O. *Int. J. Hydrogen Energy* **2011**, *36*, 4702−4709.

(106) McKone, J. R.; Sadtler, B. F.; Werlang, C. A.; Lewis, N. S.; Gray, H. B. *ACS Catal.* **2012**, *3*, 166−169.

(107) Videa, M.; Crespo, D.; GCasillas, G.; Zavala, G. *J. New Mater. Electrochem. Syst.* **2010**, *13*, 239−244.

(108) Popczun, E. J.; McKone, J. R.; Read, C. G.; Biacchi, A. J.; Wiltrout, A. M.; Lewis, N. S.; Schaak, R. E. *J. Am. Chem. Soc.* **2013**, *135*, 9267−9270.

(109) Popczun, E. J.; Read, C. G.; Roske, C. W.; Lewis, N. S.; Schaak, R. E. *Angew. Chem., Int. Ed.* **2014**, *53*, 5427−5430.

(110) Vrubel, H.; Hu, X. *ACS Catal.* **2013**, *3*, 2002−2011.

(111) Zhang, S.; Yuan, X.; Wang, H.; Mérida, W.; Zhu, H.; Shen, J.; Wu, S.; Zhang, J. *Int. J. Hydrogen Energy* **2009**, *34*, 388−404.

(112) Lin, R.; Xiong, F.; Tang, W. C.; Técher, L.; Zhang, J. M.; Ma, J. X. *J. Power Sources* **2014**, *260*, 150−158.

(113) Topalov, A. A.; Cherevko, S.; Zeradjanin, A. R.; Meier, J. C.; Katsounaros, I.; Mayrhofer, K. J. *J. Chem. Sci.* **2014**, *5*, 631−638.

(114) Borup, R.; Meyers, J.; Pivovar, B.; Kim, Y. S.; Mukundan, R.; Garland, N.; Myers, D.; Wilson, M.; Garzon, F.; Wood, D.; Zelenay, P.; More, K.; Stroh, K.; Zawodzinski, T.; Boncella, J.; McGrath, J. E.; Inaba, M.; Miyatake, K.; Hori, M.; Ota, K.; Ogumi, Z.; Miyata, S.; Nishikata, A.; Siroma, Z.; Uchimoto, Y.; Yasuda, K.; Kimijima, K.-i.; Iwashita, N. *Chem. Rev.* **2007**, *107*, 3904−3951.

(115) Hitchcock, A. P.; Berejnov, V.; Lee, V.; West, M.; Colbow, V.; Dutta, M.; Wessel, S. *J. Power Sources* **2014**, *266*, 66−78.

(116) Dhanushkodi, S. R.; Kundu, S.; Fowler, M. W.; Pritzker, M. D. *J. Power Sources* **2014**, *245*, 1035−1045.